

Phases, transitions, and patterns in the one-dimensional Extended Bose-Hubbard model

Jamshid Moradi Kurdestany* and Subroto Mukerjee†
*Centre for Condensed Matter Theory, Department of Physics,
 Indian Institute of Science, Bangalore 560 012, India*‡

Ramesh V. Pai§
Department of Physics, Goa University, Taleigao Plateau, Goa 403 206, India

Rahul Pandit¶
*Centre for Condensed Matter Theory, Department of Physics,
 Indian Institute of Science, Bangalore 560012, India.*
 (Dated: July 31, 2018)

We carry out an extensive study of the phase diagram of the extended Bose Hubbard model, with a mean filling of one boson per site, in one dimension by using the density matrix renormalization group and show that it can have Superfluid (SF), Mott-insulator (MI), density-wave (DW) and Haldane-insulator (HI) phases depending on the precise value of filling and how edge states are handled. We show that the critical exponents and central charge for the HI-DW, MI-HI and SF-MI transitions are consistent with those for models in the two-dimensional Ising, Gaussian, and Berezinskii-Kosterlitz-Thouless (BKT) universality classes, respectively; and we suggest that the SF-HI transition may be more exotic than a simple BKT transition.

I. INTRODUCTION

Over the last two decades, experiments on cold alkali atoms in traps have obtained various phases of correlated bosons and fermions [1]. Microscopic interaction parameters can be tuned in such experiments, which provide, therefore, excellent laboratories for studies of quantum phase transitions, such as those between superfluid (SF) and Mott-insulator (MI) phases in a system of interacting bosons in an optical lattice [2–4]. The SF and MI phases are, respectively, the prototypical examples of gapless and gapped phases in such systems; in addition, it may be possible to obtain other phases, e.g., density-wave (DW) [5–8], Haldane-insulator (HI) [9, 10], and supersolid (SS) [11] phases, in systems with a dipolar condensate of ^{52}Cr atoms [12]. The first step in developing an understanding of such experiments is to study lattice models of bosons with long-range interactions [13]; the simplest model that goes beyond the Bose-Hubbard model with onsite, repulsive interactions [2, 3] is the extended Bose-Hubbard model (EBHM), which allows for repulsive interactions between bosons on a site and also on nearest-neighbor sites [6, 8]. The one-dimensional (1D) EBHM is particularly interesting because (a) quantum fluctuations are strong enough to replace long-range SF order by a quasi-long-range SF, with a power-law de-

cay of order-parameter correlations [6], and (b) even a slight deviation from integer filling and the state of the boundaries play important roles here, in so far as they can modify the phase diagram [9, 10, 14, 15], in a way that is, at first glance, not possible in the thermodynamic limit [16].

The 1D EBHM is defined by the Hamiltonian

$$\mathcal{H} = -t \sum_i (a_i^\dagger a_{i+1} + H.c.) + \frac{U}{2} \sum_i \hat{n}_i (\hat{n}_i - 1) + V \sum_i \hat{n}_i \hat{n}_{i+1}, \quad (1)$$

where t is the amplitude for a boson to hop from site i to its nearest-neighbor sites, $H.c.$ denotes the Hermitian conjugate, a_i^\dagger , a_i , and $\hat{n}_i \equiv a_i^\dagger a_i$ are, respectively, boson creation, annihilation, and number operators at the site i , the repulsive potential between bosons on the same site is U , and V is the repulsive interaction between bosons on nearest-neighbor sites.

At a filling ρ of one boson per site, the phases of this model can be understood simply in the limits $(U/t, V/t) \rightarrow 0$ and $(U/t, V/t) \rightarrow \infty$. In the former limit, the hopping energy scale dominates over the interaction scales; this causes the bosons to delocalize and an SF phase is obtained. In the opposite limit, the interaction scales dominate. Two possibilities exist in this strong-coupling limit: (a) If $U > V$, the system prefers to have one boson at every site to minimize the energy costs of double and multiple occupancy, so an MI phase is stabilized; this has a gap (a charge gap if the bosons are charged) and a uniform average filling of one boson per site. (b) If $V > U$, the system prefers to have a non-uniform filling, with an average of two and zero bosons on adjacent sites, to minimize the nearest-neighbor-interaction energy, i.e., the system has a density-wave (DW) phase with wave vector $k = \pi$.

* jmkurdestany@gmail.com

† smukerjee@physics.iisc.ernet.in

‡ Also at Jawaharlal Nehru Centre For Advanced Scientific Research, Jakkur, Bangalore, India

§ rvpai@unigoa.ac.in

¶ rahul@physics.iisc.ernet.in; Also at Jawaharlal Nehru Centre For Advanced Scientific Research, Jakkur, Bangalore, India

These phases have been obtained in an early density-matrix-renormalization-group (DMRG) [6] study of the EBHM.

We now give a qualitative argument, first introduced in Ref. [9] for an EBH model with long-range interactions, which suggests that, at intermediate values of U and V , an exotic phase with a string order parameter can also be obtained. In the strong-coupling regime, the MI and DW states obtained are both, approximately, eigenstates of the site-occupation number operators for bosons; thus, they have very small boson-number fluctuations. In the intermediate-coupling range, we expect the magnitude of these fluctuations to increase. At an average filling of one boson per site, the lowest-energy number fluctuations, over the MI state, have zero or two bosons per site; similarly, the lowest-energy number fluctuations, over the DW state, have one boson per site. Thus, the intermediate-coupling-regime state, which is obtained regardless of whether we start from the MI or DW phase, is one with three possible occupancies per site, namely, 0, 1, and 2 bosons per site. We can, therefore, use an effective, spin-one model for this system at intermediate values of U and V , which are not so large that a spin-1/2 description is adequate and not so small that there is a significant probability of more than 2 bosons at a site.

In the paper in which Dalla Torre, *et al.* [9] have introduced this line of reasoning, in the context of a model of bosons with long-range interactions, they have shown, furthermore, that the effective, spin-1 model admits a Haldane-type phase, namely, the Haldane Insulator (HI). A Haldane phase, which arises in chains of integer-valued spins [17], is characterized by a gap and a nonzero string order parameter [18]. The original work of Haldane [17] has used spin systems with $SU(2)$ symmetry; it has been shown subsequently that the Haldane phase, in this case, is a state with a broken, hidden $Z_2 \times Z_2$ symmetry, and this phase can exist even in the absence of $SU(2)$ symmetry in the Hamiltonian [19]. The robustness of the Haldane phase to various types of perturbations has been investigated recently in Ref. [20].

When we map the EBH model, in the intermediate-coupling range, onto an effective, spin-1, one model, the latter does not have $SU(2)$ symmetry because of the extended-interaction term V . Nevertheless, we expect the Haldane phase to survive; and we demonstrate its existence and elucidate the conditions under which it is obtained.

The intermediate-coupling regime can also be studied by proceeding from the SF phase, which has very strong number fluctuations; these fluctuations are suppressed as the strength of the interactions is increased. In this case it might be possible to stabilize an SS phase, in which number fluctuations are not sufficiently large to localize the bosons completely (and thus destroy superfluidity), but strong enough to produce a modulation in average density. The existence of the SS phase in the EBH model needs a very careful study as we explain in detail below. However, there have been claims of the existence of an

SS phase in the EBH model [7].

In addition to identifying the various phases of the EBH model, we must also characterize the transitions between the different phases. The broken symmetries of these phases can, in principle, be used to guess the possible universality classes of the continuous transitions (as in the Landau paradigm [21]). However, it is extremely important to obtain these universality classes by direct studies, which must often be numerical, for the following two reasons: (1) Strong quantum fluctuations in one dimension can modify the natures of the transitions that might be expected on the basis of the Landau-paradigm view; and (2) energy considerations can make a first-order transition preempt a continuous transition, which we might expect naïvely in a Landau picture.

The broken symmetries in the SF and DW phases are, respectively, $U(1)$ (gauge) and Z_2 (lattice translation). The MI state breaks no symmetries; and the Haldane (HI) phase has a hidden, broken symmetry and no local order parameter. Thus, we expect the following universality classes: (A) The SF-MI transition to be in the $U(1)$ universality class appropriate for a one-dimensional quantum system (the Berezinski-Kosterlitz-Thouless (BKT) transition in the two-dimensional (2D) XY model), like in the usual Bose-Hubbard model. (B) The MI-DW transition should be in the 2D, Z_2 (Ising) universality class. (C) The SF-DW transition involves two different order parameters, so it should have both BKT and 2D Ising characters. These expectations have, indeed, been confirmed in a previous work [6].

The phase transitions involving the new HI phase, which we study here, have not been accurately characterized so far. The HI phase has no local order parameter, so the transitions into this phase, from the other phases, may be exotic. We expect the HI-DW transition to have 2D Ising character, because the DW phase has long-range order, with a well-defined local order parameter. We might, at first sight, expect the SF-HI transition to be of the BKT type; but the interplay of quasi-long-range order, in the SF phase, and the string correlations, in the HI phase, might lead to an exotic transition. The MI-HI transition is perhaps the most interesting transition in the EBH model, because both phases have gaps and no local order parameter; in addition, the HI phase is characterized by a string order parameter. The field theory of this transition has been studied in Ref. [10]; and a similar transition, in a spin-1 model, has been studied numerically in Ref. [22]. This transition has been argued to be in the Gaussian universality class, which has continuously varying critical exponents and was first studied in models of roughening [23]. In this work, we perform extensive numerical studies to elucidate the natures of these transitions.

We present density-matrix-renormalization-group (DMRG) [6] studies of the phases, transitions, and the role of boundaries in the 1D EBHM with a mean filling of one boson per site. Although a few DMRG studies [6, 9, 10, 14, 15] have been carried out earlier, none of

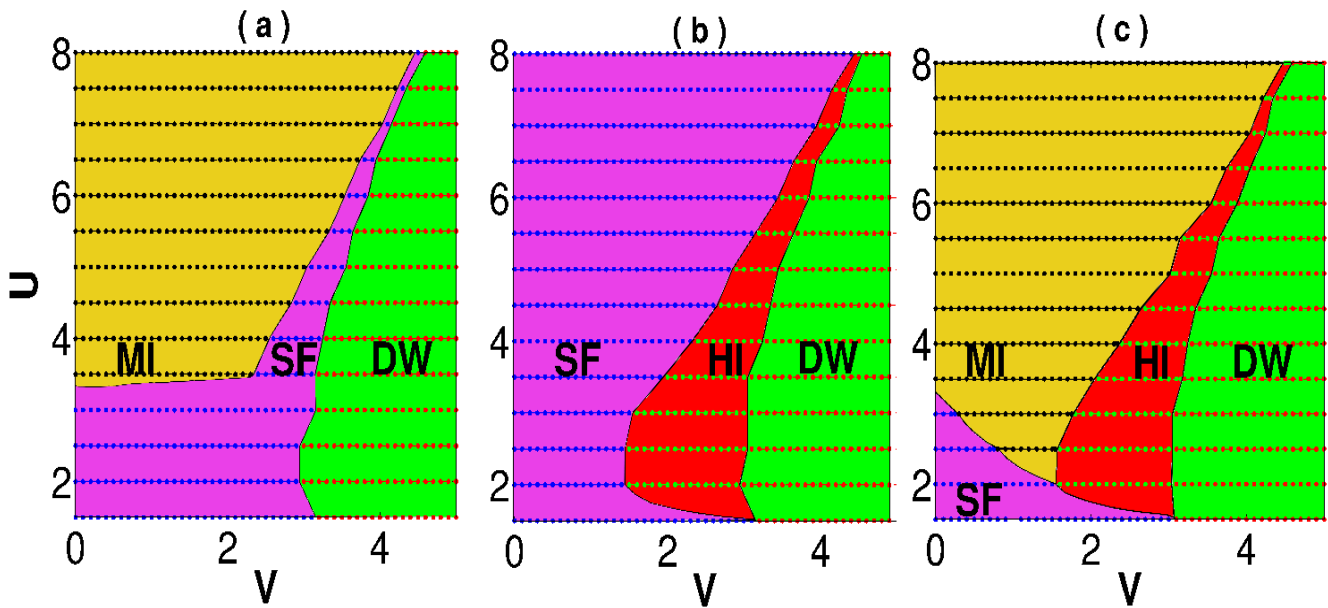


FIG. 1. (Color online) Phase diagrams in the (U, V) plane for the 1D EBHM with the following constraints (a) T1 ($N = L$), (b) T2 ($N = L + 1$), and (c) T3 ($N = L$) and $\mu_r = -\mu_l = 2$ showing Mott-insulator (MI ochre), superfluid (SF purple), Haldane-insulator (HI red), and density-wave (DW green) phases and the phase boundaries between them; in this range of U and V all transitions are continuous; at larger values of U and V the MI-DW and HI-DW transitions become first-order.

them has elucidated completely clearly the universality classes of the continuous transitions in the 1D EBHM; nor have they compared in detail, the phase diagrams of this model with different types of boundaries and filling. Our study, which has been designed to obtain the universality classes of these transitions and to examine the roles of boundary states and filling in stabilizing different phases, yields a variety of interesting results that we summarize qualitatively below: If the filling $\rho = 1$, in the thermodynamic limit, we obtain three types of phase diagrams, P1 (Fig. 1(a)), P2 (Fig. 1(b)), and P3 (Fig. 1(c)), for the following three different types of constraints on the system: T1 (number of bosons $N = L$, where L is the number of sites); T2 ($N = L + 1$); and T3 ($N = L$ and additional chemical potentials at the boundary sites, as we describe below). For P1 we obtain SF, MI, and DW phases and we confirm, as noted earlier [6], that the SF-MI transition is in the BKT [24] universality class and the SF-DW has both BKT and 2D Ising characteristics; at sufficiently large values of the repulsive parameters, the MI-DW transition is of first order [6]. The phase diagram P2 displays SF, HI, and DW phases, with continuous SF-HI and HI-DW transitions in BKT and 2D Ising universality classes, respectively. The phase diagram P3 has SF, MI, HI, and DW phases, with SF-MI, MI-HI, HI-DW in BKT, 2D Gaussian [22], and 2D Ising universality classes, respectively; the SF-HI transition is more exotic than a simple BKT transition; at sufficiently large values of the repulsive parameters, there is a first-order MI-DW phase boundary.

The remaining part of this paper is organized as fol-

lows. In Sec. II we give details of the EBH model and define the quantities we calculate. Section III is devoted to our results. Sec. IV contains concluding remarks. The details of the DMRG we use are given in the Appendix.

II. MODEL

We set the scale of energies by choosing $t = 1$. We work with a fixed value of the filling ρ and focus on $\rho = 1$, i.e., a filling of one boson per site in the thermodynamic limit, which we realize in three different ways, to highlight the role of filling and boundary states, by using the three different constraint conditions T1, T2, and T3. In all these three cases, we have open boundaries; in T3, we include boundary chemical potentials $\mu_l = -2t$ and $\mu_r = 2t$ at the left and right boundaries, which are denoted by the subscripts l and r , respectively. We study this model by using the DMRG method that has been described in Ref.[6] (see also the Appendix). To characterize the phases and transitions in this model, we calculate the following thermodynamic and correlation functions and the entanglement entropy (familiar from quantum infor-

mation):

$$\begin{aligned}
R_{dw}(|i-j|) &= (-1)^{|i-j|} \langle \delta \hat{n}_i \delta \hat{n}_j \rangle, \\
R_{string}(|i-j|) &= \langle \delta \hat{n}_i e^{i\pi \sum_{l=i}^j \delta \hat{n}_l} \delta \hat{n}_j \rangle, \\
R_{SF}(|i-j|) &= \langle a_i^\dagger a_j \rangle, \\
\mathcal{S}_\pi &= \sum_{i,j=1}^L e^{i\pi(i-j)} \langle \hat{n}_i \hat{n}_j \rangle / L^2, \\
n(k=0) &= \sum_{i,j}^L \langle a_i^\dagger a_j \rangle / L, \\
G_L^{NG} &= E_L^1(N) - E_L^0(N), \\
G_L^{CG} &= E_L^0(N+1) + E_L^0(N-1) - 2E_L^0(N), \\
\xi_L &= \sqrt{\frac{\sum_{i,j=1}^L (i-j)^2 \langle a_i^\dagger a_j \rangle}{\sum_{i,j=1}^L \langle a_i^\dagger a_j \rangle}}, \\
S_L(l) &= - \sum_i^{n_{states}} \lambda_i \log_2 \lambda_i, \\
F &= LG_L^{CG} \left(1 + \frac{1}{2 \ln L + B} \right), \\
D &= \ln L - a|V - V_c|^{-1/2}, \tag{2}
\end{aligned}$$

where $\delta \hat{n}_i = \hat{n}_i - \rho$, the correlation functions for the DW, HI, and SF phases are $R_{dw}(|i-j|)$, $R_{string}(|i-j|)$, $R_{SF}(|i-j|)$, respectively, \mathcal{S}_π is the density-density structure factor at wave number $k = \pi$, $n(k=0)$ the momentum distribution of the bosons at $k=0$, G_L^{NG} and G_L^{CG} are neutral and charge gaps [25], $E_L^0(N)$ and $E_L^1(N)$ are the ground-state and first-excited-state energies, respectively, for our system with L sites and N bosons, ξ_L is a system-size-dependent correlation length; $S_L(l)$ is the von-Neumann block entanglement entropy, λ_i , the eigenvalues of the reduced density matrix for the right block, of length l , which yield the entanglement spectrum in our DMRG [6], and n_{states} is the number of states that we retain for this density matrix; note that $S_L(l) = c\lambda$ at a critical point [26], with c the central charge and the log-conformal distance $\lambda = (\log[\frac{2L}{\pi} \sin(\frac{\pi l}{L})])/6$; a and B depend on the critical value V_c , at which the concerned transition occurs; V_c depends on U . The order parameters for the DW and HI phases are $O_{dw} = \sqrt{\lim_{|i-j| \rightarrow \infty} R_{dw}(|i-j|)}$ and $O_{string} = \sqrt{\lim_{|i-j| \rightarrow \infty} R_{string}(|i-j|)}$, respectively; for the DW, HI and SF phases, we also use the Fourier transforms of the correlation functions, which we denote by $R_{dw}(k)$, $R_{string}(k)$, $R_{SF}(k)$, respectively. Our calculations have been performed with $100 \leq L \leq 300$, a maximal number $n_{max} = 6$ of bosons at a site, and up to $n_{states} = 256$ states in our density matrices; we have checked, in representative cases, that, for the ranges of U and V we cover, our results are not affected significantly if we use $n_{max} = 4$ and $n_{states} = 128$; for the MI-HI transition we have also used $L = 1024$.

III. RESULTS

In Figs. 1 (a), (b), and (c) we depict our DMRG phase diagrams, in the (U, V) plane, for the 1D EBHM with constraints T1, T2, and T3, respectively. These phase diagrams show MI (ochre), SF (purple), HI (red), and DW (green) phases and the phase boundaries between them; the points inside these phases indicate the values of U and V for which we have carried out our DMRG calculations. In the ranges of U and V that we consider here, all transitions are continuous; at larger values of U and V than those shown in Fig. 1, the MI-DW transitions become first-order, as shown for T1 in Ref.[6]; the direct MI-DW transition, at large values of U and V , is also of first order with the T3 constraint. Note that MI (HI) phases appear with conditions T1 and T3 (T2 and T3). The MI phase occurs at a strict commensurate filling (T1 with $N = L$) and is characterized by a charge gap, which arises because of the onsite interaction U that penalizes the presence of more than one boson at a site. With the constraint T2, $N = L + 1$, so there is one more boson in the system than in case T1; this extra boson can hop over the commensurate, T1, MI state, produce gapless excitations in the upper Mott-Hubbard band, and thereby destroy the MI phase, which is replaced by SF or HI phases.

The origin of the HI phase in the 1D EBHM has been elucidated in the Introduction. This phase also has gapless edge modes, which destroy the charge gap at strict commensurate filling (T1). However, with an extra boson (T2), these gapless modes get quenched, so we obtain an HI phase with a gap. At strict commensurate filling, we can gap out the edge modes by applying boundary chemical potentials μ_l and μ_r (T3). This allows us to obtain the HI phase and also the MI phase. A similar procedure was used in the study of integer spin chains [27]. Note also that the HI phase exists because of boson-number fluctuations about the Mott state; so we expect the HI to give way to the MI phase at large values of U at which such number fluctuations are suppressed, in much the same way as the SF yields to the MI at large values of U . In the large- U and large- V regions, which we do not show in the phase diagrams of Fig. 1, there is a direct, first-order, MI-DW transition [6].

We now obtain the universality classes of the continuous transitions in the phase diagrams of Fig. 1. It has been noted in Ref.[6] that the MI-SF transition in Fig. 1 (a), with the constraint T1, is in the Berezinskii-Kosterlitz-Thouless (BKT) class, whereas the SF-DW has both BKT and 2D Ising characters, in as much as the SF correlation length shows a BKT divergence but the DW order parameter decays to zero with a 2D-Ising, order-parameter exponent; this transition should be in the universality class of the Wess-Zumino-Witten $SU(2)_1$ theory like the critical point that lies between the BKT phase and the antiferromagnetic phase in the spin-1/2, XXZ antiferromagnetic chain [28]. The MI-SF and SF-DW phase boundaries in Fig. 1 (a) merge, most probably

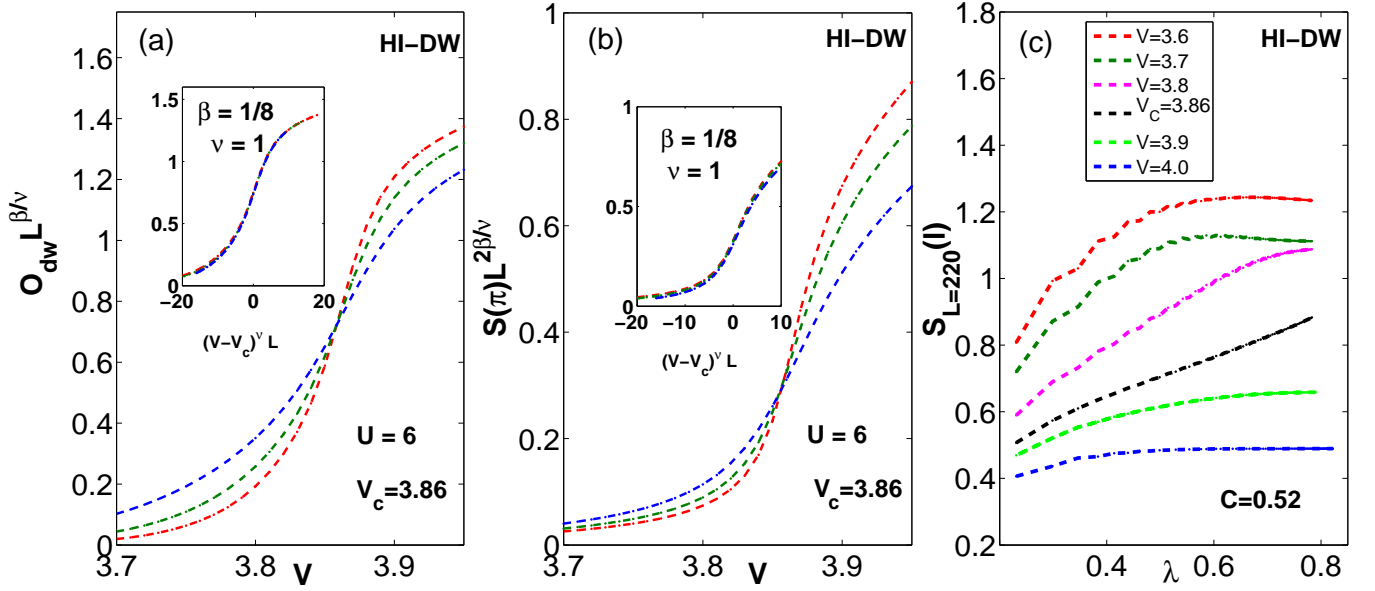


FIG. 2. (Color online) Plots for the HI-DW transition at $U = 6$, with $L = 200$ (red curve), $L = 150$ (green curve), and $L = 100$ (blue curve), of (a) the scaled DW order parameter $O_{dw} L^{\beta/\nu}$ versus V (the inset shows $O_{dw} L^{\beta/\nu}$ versus $(V - V_c)^\nu L$, where β and ν are order-parameter and correlation-length exponents, (b) the $k = \pi$ scaled structure factor $S(\pi) L^{2\beta/\nu}$ versus V (the inset shows $S(\pi) L^{2\beta/\nu}$ versus $(V - V_c)^\nu L$), and (c) the block entanglement entropy $S_L(l)$ versus the logarithmic conformal distance $\lambda = \frac{1}{6} \log[\frac{2L}{\pi} \sin(\frac{\pi l}{L})]$ for an open system of length $L = 220$ for different values of V (the slope of the linear part of the curve for $V_c = 3.86$ yields a central charge $c = 0.52$). The system is of type T3.

at a bicritical point, beyond which the MI-DW transition is first order [6]. We concentrate here on the HI-SF, HI-DW, and HI-MI transitions, all of which can be found in Fig. 1 (c), with the constraint T3, for which we present results in Figs. 2, 3, 4 and 5; we have checked explicitly that the universality classes of the HI-SF and HI-DW transitions are the same for both types of constraints T2 and T3.

In Fig. 2 (a) we plot the scaled DW order parameter $O_{dw} L^{\beta/\nu}$ versus V near the representative point, $V_c \simeq 3.86$ and $U = 6$, on the HI-DW phase boundary for $L = 200$ (red curve), $L = 150$ (blue curve), and $L = 100$ (green curve); the inset gives a plot of $O_{dw} L^{\beta/\nu}$ versus $(V - V_c)^\nu L$; Fig. 2 (b) presents a similar plot and inset for the scaled structure factor $S(\pi) L^{2\beta/\nu}$ at wave number $k = \pi$; in Fig. 2 (c) we plot the von-Neumann block entanglement entropy $S_L(l)$ versus the logarithmic conformal distance λ for $L = 220$ and a range of values of V in the vicinity of $V_c(U = 6) = 3.86$. The values of the exponents β and ν and the value of the central charge c that we obtain from Figs. 2 (a) – (c), namely, $\beta = 1/8$, $\nu = 1$, and $c = 0.52$, are consistent with their values in 2D Ising model. If we restrict the occupancy to one boson per site, in the limit $U, V \rightarrow \infty$ with fixed U/V , the DW state can be represented as $|\dots 20202020\dots\rangle$ in the site-occupancy basis; this state is doubly degenerate and clearly breaks the translational symmetry of the lattice by doubling the unit cell; in contrast, the HI state has the translational invariance of the lattice. Given this double degeneracy of the DW state, we expect that, if the HI-DW transition

is continuous, it should be in the 2D Ising universality class; as we have shown above, our DMRG results for the HI-DW transition in the 1D EBHM are consistent with this expectation. Note that the string order parameter O_{string} is nonzero in both the HI and DW phases; thus, it is not the order parameter that is required for identifying the universality class of the HI-DW transition. We find, furthermore, the string-order-parameter correlation length is so large in the HI phase that, given the values of L in our study, it is not possible to get a reliable estimate for this correlation length.

To investigate the critical behavior of the MI-HI transition, we plot $R_{string}(k = 0) L^{2\beta/\nu}$ versus V , in Fig. 3 (a), whose inset shows a plot of $R_{string}(k = 0) L^{2\beta/\nu}$ versus $(V - V_c)^\nu L$. These scaling plots indicate that, for $U = 6$, the MI-HI critical point is at $V_c \simeq 3.5$ with exponents $\beta = 0.35$ and $\nu = 1.18$; this value of β is consistent with the Gaussian-model [22] (superscript G) result $\beta^G = 1/\sqrt{8}$. Our value for ν follows from the plot of L/ξ_L versus V in Fig. 3 (b), whose inset shows a plot of L/ξ_L versus $(V - V_c) L^{1/\nu}$. For the central charge we obtain $c = 1.02$, which is consistent with $c^G = 1$ given our error bars, from the plot of $S_L(l)$ versus λ for $L = 220$ in Fig. 3 (c). As we have mentioned above, for large U we can restrict the occupancies in the 1D EBHM to 0, 1, and 2 bosons per site to obtain a spin-1 model. The analog of the MI-HI transition in this spin-1 model has been shown to be in the Gaussian universality class [22], which has a fixed exponent $\beta = 1/\sqrt{8}$ and central charge $c = 1$, but

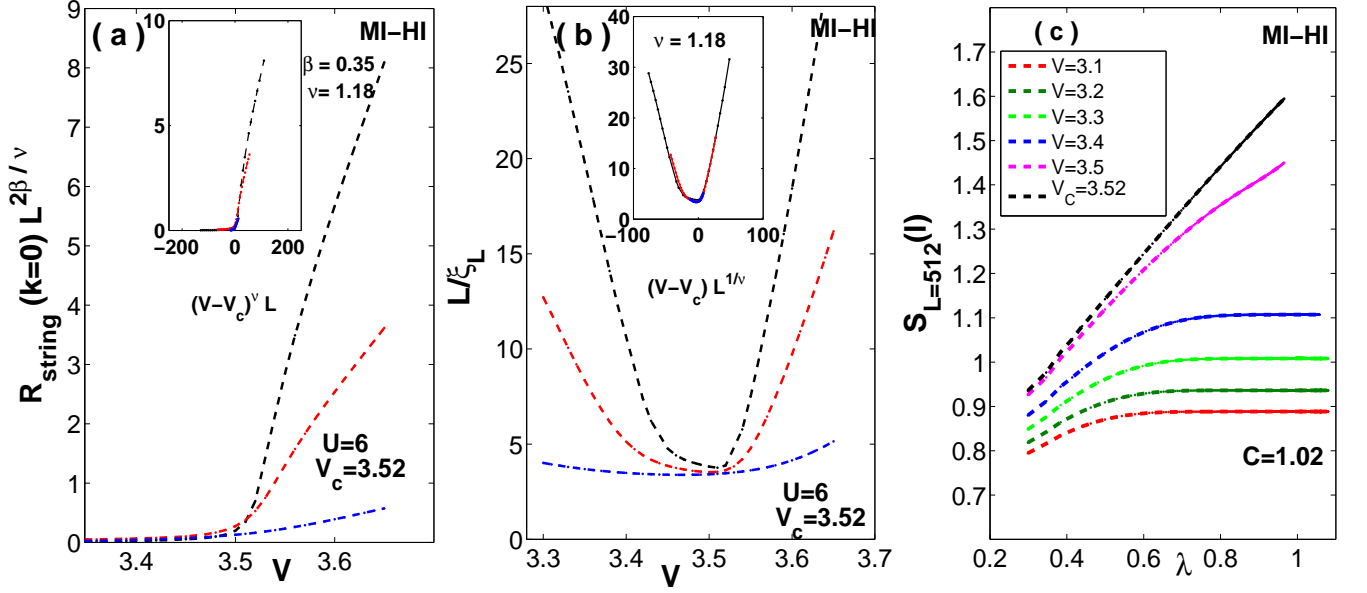


FIG. 3. (Color online) For this particular phase transition, we used lengths up to $L = 1024$ to calculate the critical point, central charge, and critical exponents; the values for these exponents do not change significantly if we use lengths up to $L = 290$. (a)-(c) show the analogs, for the MI-HI transition, of the plots in Figs. 2 (a)-(c) for the HI-DW transition but with (a) $O_{dw} L^{\beta/\nu}$ replaced by $R_{string}(k=0) L^{2\beta/\nu}$, the scaled Fourier transform of string correlation function at $k=0$, and (b) $S(\pi) L^{2\beta/\nu}$ replaced by L/ξ_L ; in (a) and (b) the values of L are 1024 (black curve) 512 (red curve), and 128 (blue curve). The system is of type T3.

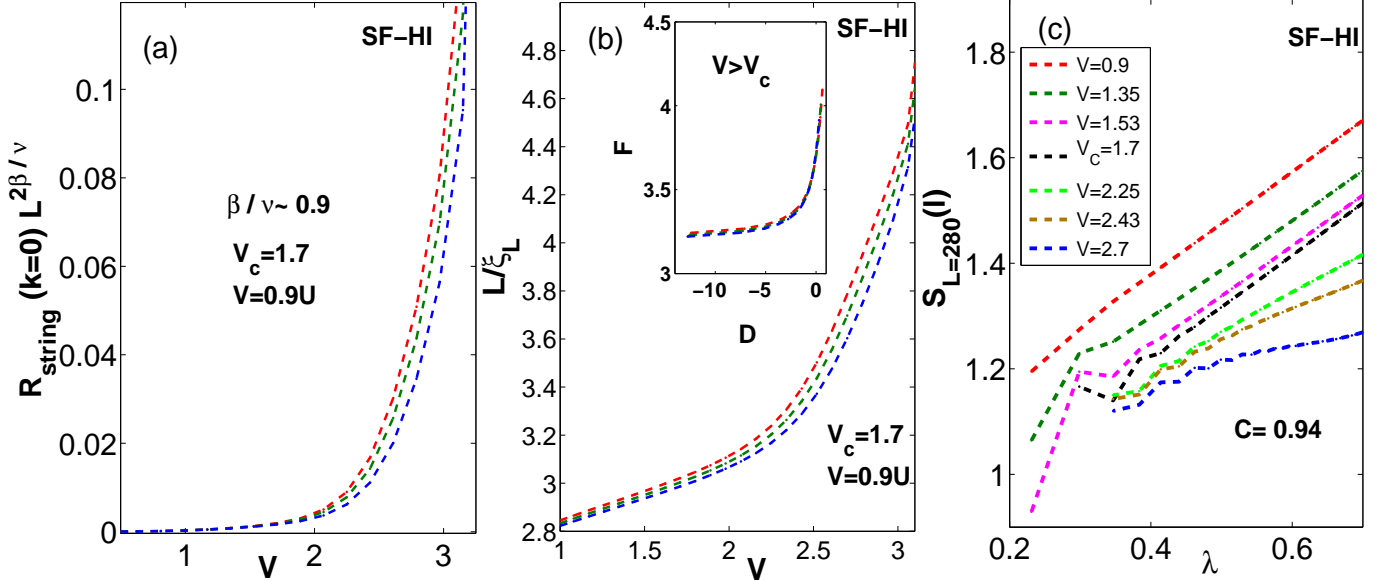


FIG. 4. (Color online) (a)-(c) show the analogs, for the SF-HI transition, of the plots in Figs. 3 (a)-(c) for the MI-HI transition (the inset in (b) shows a plot of the scaled charge gap F versus D (see Eq. 2); in (a) and (b) the values of L are 280 (red curve) 240 (green curve), and 200 (blue curve). The system is of type T3.

an exponent ν that changes continuously along the phase boundary. We find indeed, from calculations like those presented in Figs. 3 (a) – (c), that β and c do not change as we move along our MI-HI phase boundary in Fig. 1 (c), but ν does; we obtain, in particular, $\nu = 1.18$, 1.22, and

1.36 for $U = 6, 5$, and 4, respectively. For this particular phase transition, we have used lengths up to $L = 1024$ to calculate the critical point, central charge, and critical exponents; the values for these exponents do not change significantly if we use lengths up to $L = 290$.

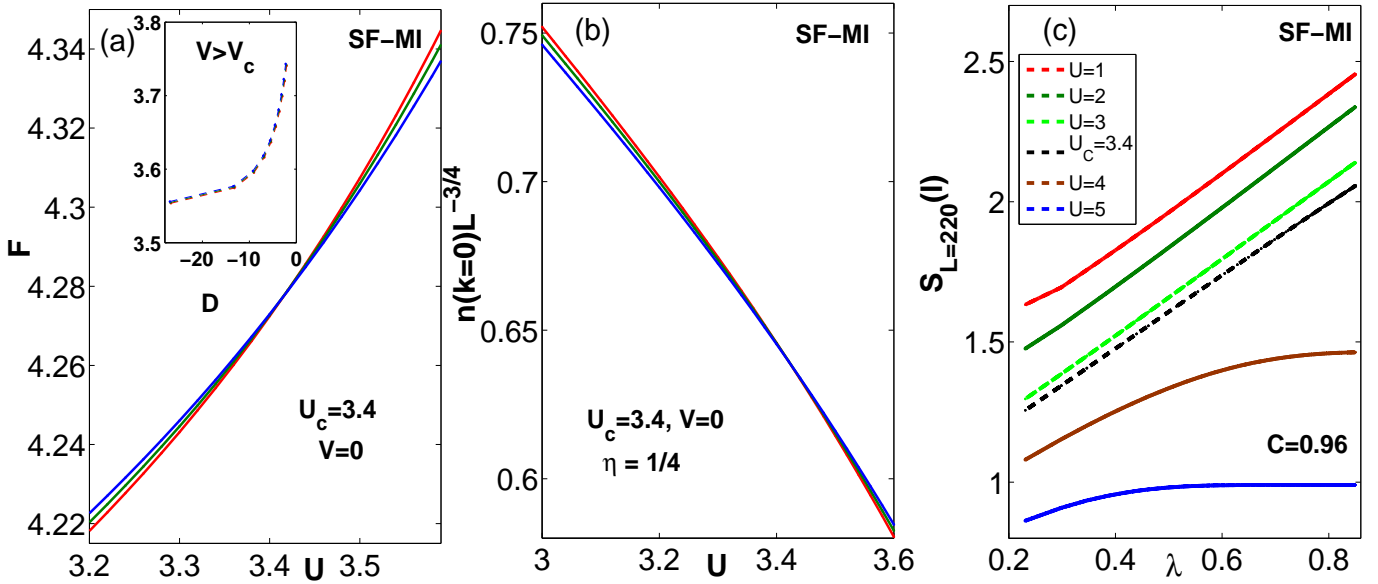


FIG. 5. (Color online) (a)-(c) show the analogs, for the SF-MI transition, of the plots in Figs. 3 (a)-(b) for the MI-HI transition but with (a) $R_{string}(k=0)L^{2\beta/\nu}$ replaced by the scaled charge gap F and V replaced by U and (b) L/ξ_L replaced by $n(k=0)L^{-3/4}$; in (a) L is 200 (red curve) 180 (green curve), 160 (blue curve) and in (b) L is 250 (red curve) 230 (green curve), and 210 (blue curve). The system is of type T3.

The critical behavior of the SF-HI transition follows from the plot of $R_{string}(k=0)L^{2\beta/\nu}$ versus V , in Fig. 4 (a), and the plot of L/ξ_L versus V , in Fig. 4 (b), whose inset shows a plot of F versus D (see Eq. 2). These scaling plots indicate that, for $V = 0.9U$, the SF-HI critical point is at $V_c \simeq 1.7$, where the correlation length diverges with an essential singularity as it does at a BKT transition [24]. Thus, we cannot define the exponent ν ; however, we can define the exponent ratio β/ν , which governs how rapidly the string order parameter vanishes as we approach the SF-HI phase boundary from the HI phase; for this ratio we obtain the estimate $\beta/\nu \simeq 0.9$. We find the central charge $c = 0.94$, which is consistent with $c = 1$ given our error bars, from the plot of $S_L(l)$ versus λ for $L = 280$ in Fig. 4 (c). The field theory for this SF-HI transition is likely to be non-standard because the SF phase has algebraic $U(1)$ order, whereas the HI phase has a non-local, string order parameter. An example of a similar transition is found in the phase diagram of the bilinear-biquadratic spin-1 chain, in which the Haldane phase (the analog of the HI phase here) undergoes a transition to a critical phase, as we change the ratio of the bilinear and biquadratic couplings; this transition is known to be described by an $SU(3)_1$ Wess-Zumino-Witten theory [29]. The gapless phase in our model is quite different from that in the spin-1 chain; and there is no $SU(3)$ symmetry at the SF-HI transition in the 1D EBHM. Nevertheless, it is likely that the SF-HI phase transition in our model is of a non-standard type, which is similar to, but not the same as, the $SU(3)_1$ theory mentioned above; this point requires more detailed in-

vestigations that lie beyond the scope of our work. Note, furthermore, that the SF-HI transition here is not fine-tuned, unlike the one above in the spin-1 chain with bilinear and biquadratic couplings, in so far as it occurs along an entire boundary in the phase diagram (Fig. 1 (c)).

For the sake of completeness, we also show, for the constraint T3, the BKT nature of the SF-MI transition in Fig. 1 (c), as noted for the T1 case in [6], by presenting plots of the scaled charge gap F versus D (see Eq. 2), the $k=0$ value of $n(k=0)$, and the block entanglement entropy $S_L(l)$ versus the log-conformal distance λ in Figs. 5 (a), (b) and (c), respectively. These plots demonstrate that, at the MI-SF transition, the correlation length (or inverse charge gap) has a BKT-type essential singularity (Figs. 5 a), the SF-correlation-function exponent $\eta = 1/4$, and the central charge is $c = 0.96$, which is consistent with $c^{BKT} = 1$ given our error bars. It is difficult to give precise error bars for the exponents and central charges that we have calculated because there are systematic errors, which include those associated with the finite values of n_{max} and n_{states} ; these errors are hard to estimate.

Our DMRG study can also be used to obtain profiles of the number of bosons n_i at a site i . Illustrative plots are given in Figs. (6) and (7) for a variety of constraints. We expect the boson number to be constant across the system in the SF, HI and MI phases and to display a modulation in the DW phase. Fig. (6) shows a plots of n_i vs i for the system at $U = 6$ with the constraints T_1 , T_2 and T_3 . It can be seen that n_i is, indeed, constant in

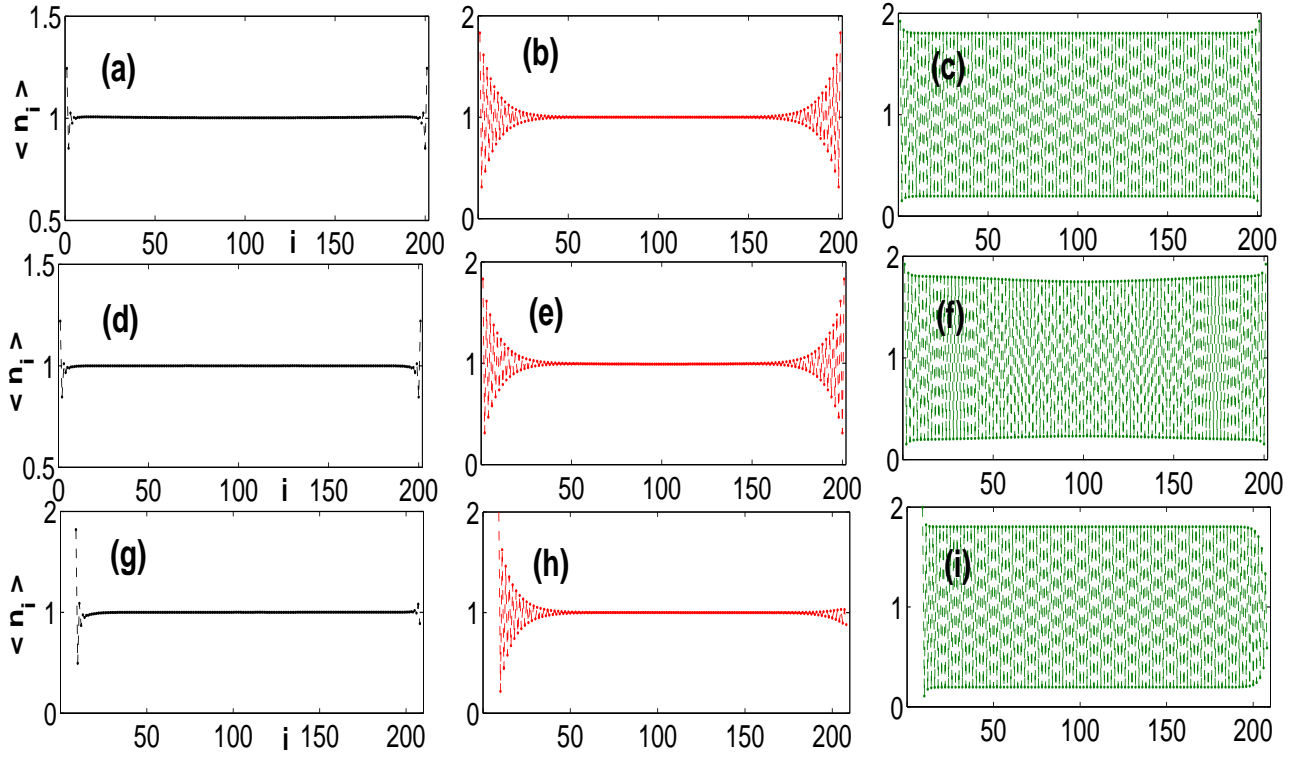


FIG. 6. (Color online) Plots of n_i versus i for the system at $U = 6$ with the constraints T_1 ((a)-(c)), T_2 ((d)-(f)), and T_3 ((g)-(i)). In (a), (d) and (g), $V = 2.5$, in (b), (e) and (h) $V = 3.7$, and in (c), (f) and (i) $V = 4.1$.

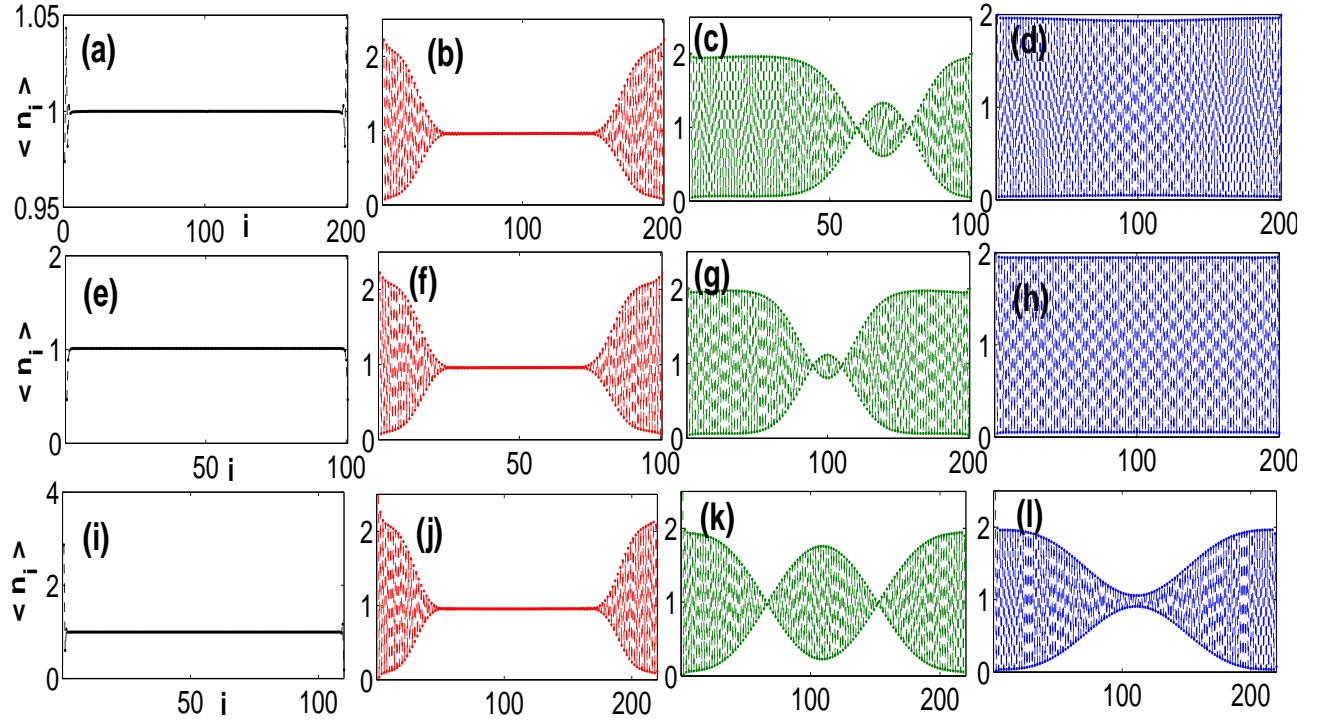


FIG. 7. (Color online) Plots of n_i versus i for the system at smaller values of $U (\approx 1)$, with the constraints T_1 ((a)-(d)), T_2 ((e)-(h)) and T_3 ((i)-(l)). In (a), (e) and (i) $V = 1$, in (b)-(j), $V = 3.5$, in (c)-(k), $V = 4.4$ and in (d)-(l) $V = 5$.

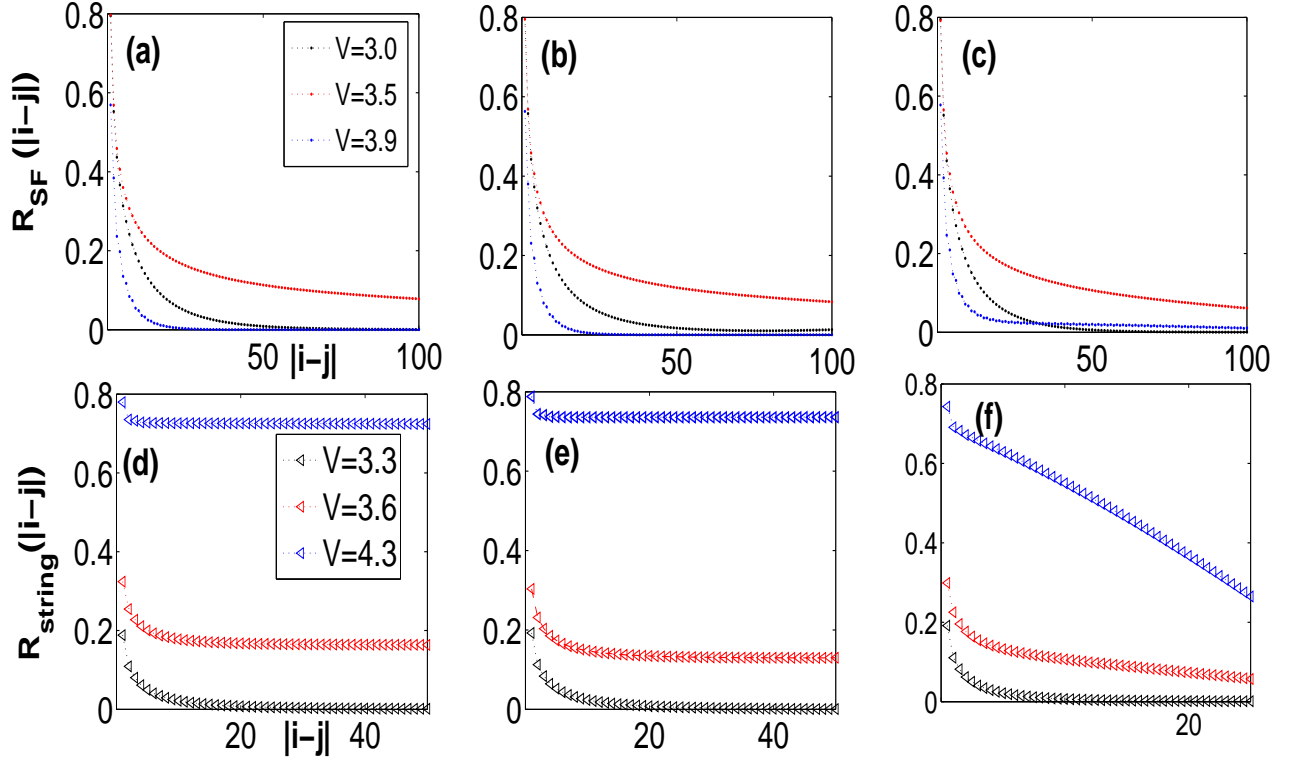


FIG. 8. (Color online) Illustrative plots of SF ((a)-(c)) and string correlation functions ((d)-(f)) for the constraints T3 ((a) and (d)), T2 ((b) and (e)), and T1 ((c) and (f)), for $U = 6$.

the MI phase (away from the boundaries) and displays modulations in the DW phase; however, there also appear to be some modulations in SF and HI phases near the DW phase for the following reasons: (A) proximity to the DW phase; and (B) the effects of open boundaries (compounded, in the HI phase, by the presence of edge modes). In fact, it can be seen that the application of edge potentials to quench the edge states suppresses the modulation on one side (with the lower chemical potential) and enhances it on the other side. The presence of this modulation, even in the SF and HI phases, prevents a very accurate determination of the phases and transitions from inspections of plots of n_i versus i ; therefore, we require other diagnostics to map out the phase diagrams accurately.

Figure. (7) shows that, at small values of $U (\simeq 1)$, where there are no MI and HI phases, but possibly an SS phase, the density modulations in the SF phase get stronger with a region of uniform density sandwiched between regions of strong modulation. A calculation that considers the entire system yields, therefore, both nonzero superfluid density and density modulation. It is tempting to conclude, on the basis of the n_i versus i plots in Fig. (7), that the system displays phase separation between the DW and SF phases and is, therefore, not in the SS phase. However, this apparent phase separation could be an artifact of the open boundaries and system sizes we employ; hence, we do not make any assertions about the existence, or lack thereof, of the SS phase. An

unambiguous resolution of this issue requires, perhaps, a DMRG calculation at fixed values of the chemical potential μ and not at a fixed mean density of bosons per site. Such a DMRG calculation lies beyond the scope of our study here.

We have also obtained various correlation functions in MI, SF, HI, and DW phases. We give some illustrative plots of SF and string correlation functions in Fig.(8) for the constraints T1, T2 and T3. These show that (a) SF correlations decay exponentially in MI, HI, and DW phases but algebraically (as power laws) in the SF phase and (b) string correlations decay to zero exponentially in SF and MI phases, but asymptote to nonzero values in the HI and DW phases.

In Fig.(9) we show plots of the charge gap (multiplied by the length L of the system); and in Fig.(10) we show plots of the neutral gap for several of the transitions in our model and for different constraints. At such transitions, one of these gaps vanishes if the transition is continuous, so the curves for different values of L (in plots such as those of Figs.(9) - (10)) cross at the transition; this can be used to detect and characterize these transitions. In particular, the HI-DW is associated with the vanishing of the neutral gap alone, whereas HI-MI transitions (Fig.(10)) are associated with the vanishing of the neutral and charge gaps.

We now show representative plots of the static von-Neumann block entropy $S_L(l)$ (Figs.(11) - (13)) versus the left-block length l (left panels) and the logarithm-

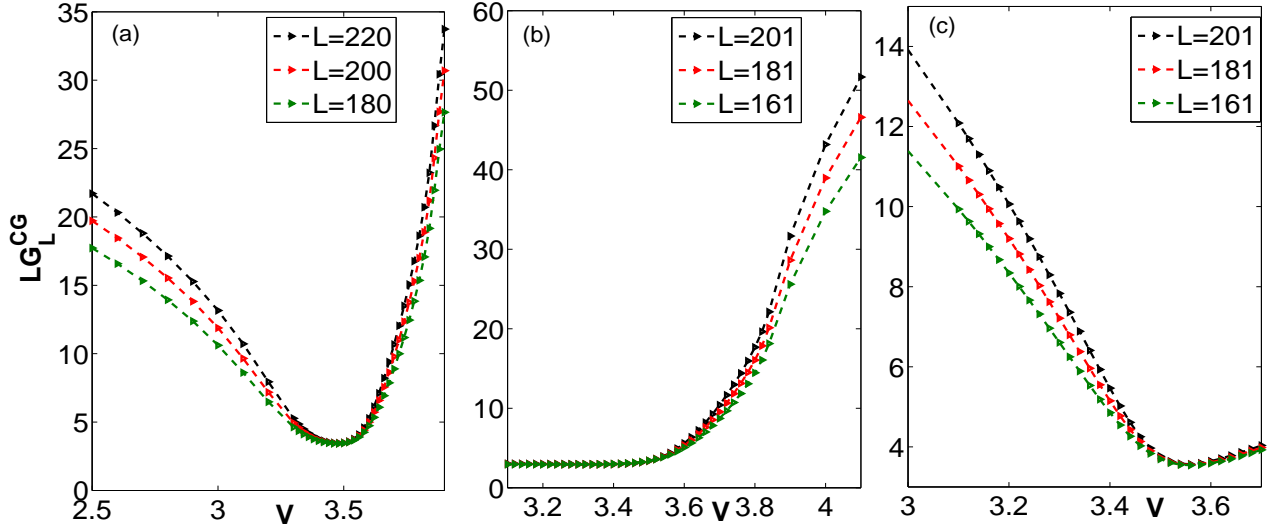


FIG. 9. (Color online) L times the charge gap for $U = 6$ and different lengths for the system with constraints (a) T3, (b) T2, and (c) T1. For T3, the gap is non zero in the MI phase at small values of V , vanishes at a point corresponding to the transition from MI to HI and then opens up again in the HI phase. For T2, the MI phase does not exist and it is replaced by a gapless SF at small V , which then gives way to the HI phase, where a gap opens up. For T1, there is a gapped MI at small V , which gives rise to an SF phase with no gap. The gap closes not just at a point (for T3) but over a range of values of V . Note that the charge gap does not go to zero at the HI-DW transition.

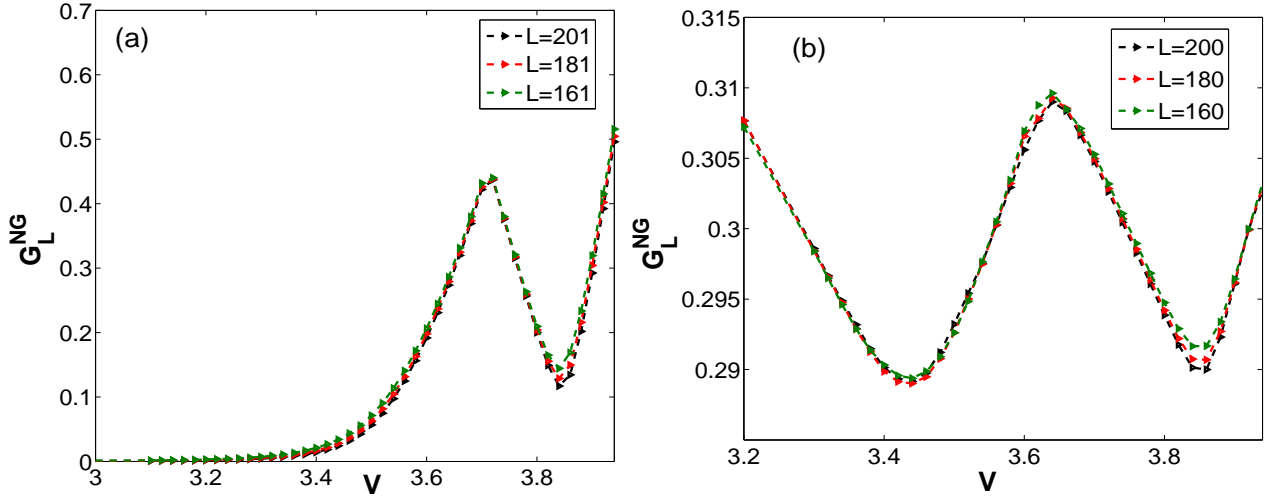


FIG. 10. (Color online) (a) The neutral gap versus V , for $U = 6$, different lengths, and the constraint T2. The neutral gap is zero in the SF phase and opens up in the HI phase and, unlike the charge gap, closes at the HI-DW transition and then opens up again in the DW phase. (b) The neutral gap versus V , for $U = 6$, different lengths, and the constraint T3.

mic conformal distance $\lambda = \frac{1}{6} \log[(2L/\pi) \sin(\pi l/L)]$ (right panels) for a variety of parameter values and constraints. In the plots versus the logarithmic conformal distance λ , linear behaviors of the curves at certain values of parameters, such as V , reveal critical points; the slopes of these lines yield the central charge c at the critical point in question. The rapid saturation of the block entropy versus λ , for other values of V , is a consequence of the short correlation length in phases such as the DW and MI phases; if the correlation length is finite, but long,

this saturation can be slow (as, e.g., in some of the plots in the HI regime). We also show, for T1-T3 constraints, plots of the entropy as a function of V ; as $L \rightarrow \infty$, such a curve can show a jump close to the Gaussian critical point $V \simeq 3.52$; and, in this limit, the curves for different values of L can converge to a step function at the 2D-Ising-type critical point at $V \simeq 3.84$ (see Fig.(14)).

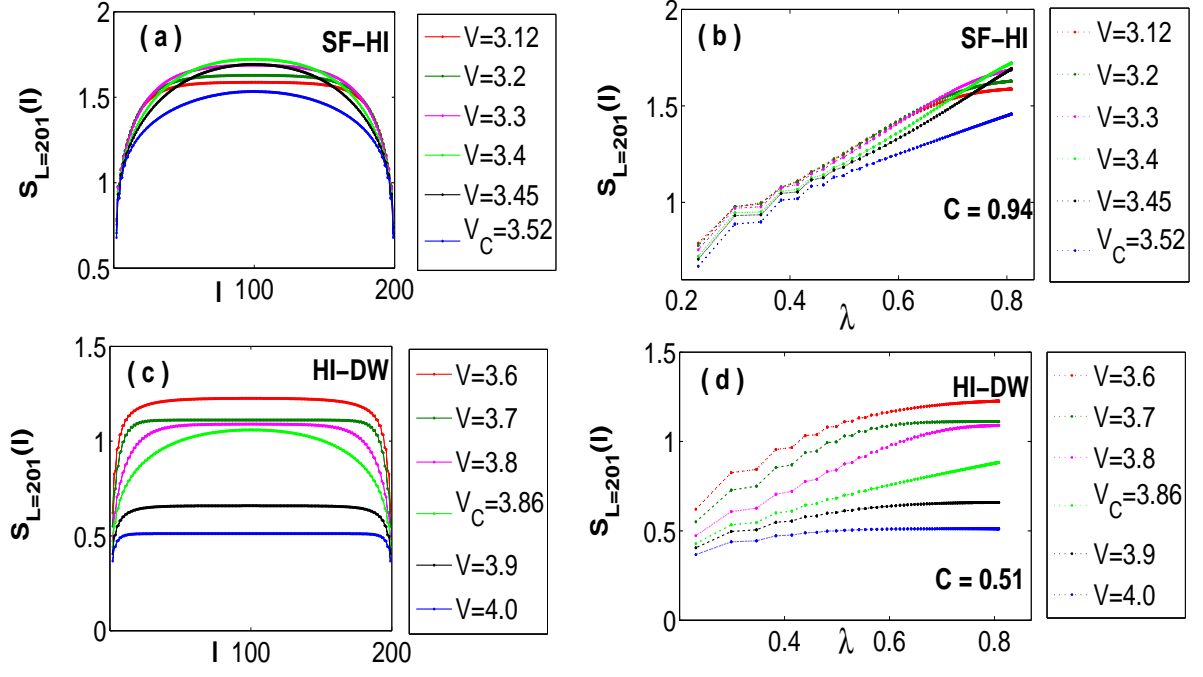


FIG. 11. (Color online) Left panels (a) and (c): the static von Neumann block entropy $S_L(l)$ for an open system of length $L = 201$ and a range of different interaction values V , located in the SF-HI and the HI-DW phases. Right panels (b) and (d): the same block entropies as a function of the logarithmic conformal distance $\frac{1}{6}\log[(2L/\pi)\sin(\pi l/L)]$; the linear behaviors of the curves for $V = 3.52$ and 3.86 reveal critical points (see text) with central charges $c \sim 1$ and $c \sim 0.5$. The rapid saturation of the entropy for other values of V is a consequence of the short correlation length in the DW and HI insulating phases. Here the average filling is 1 and we use the constraint T2.

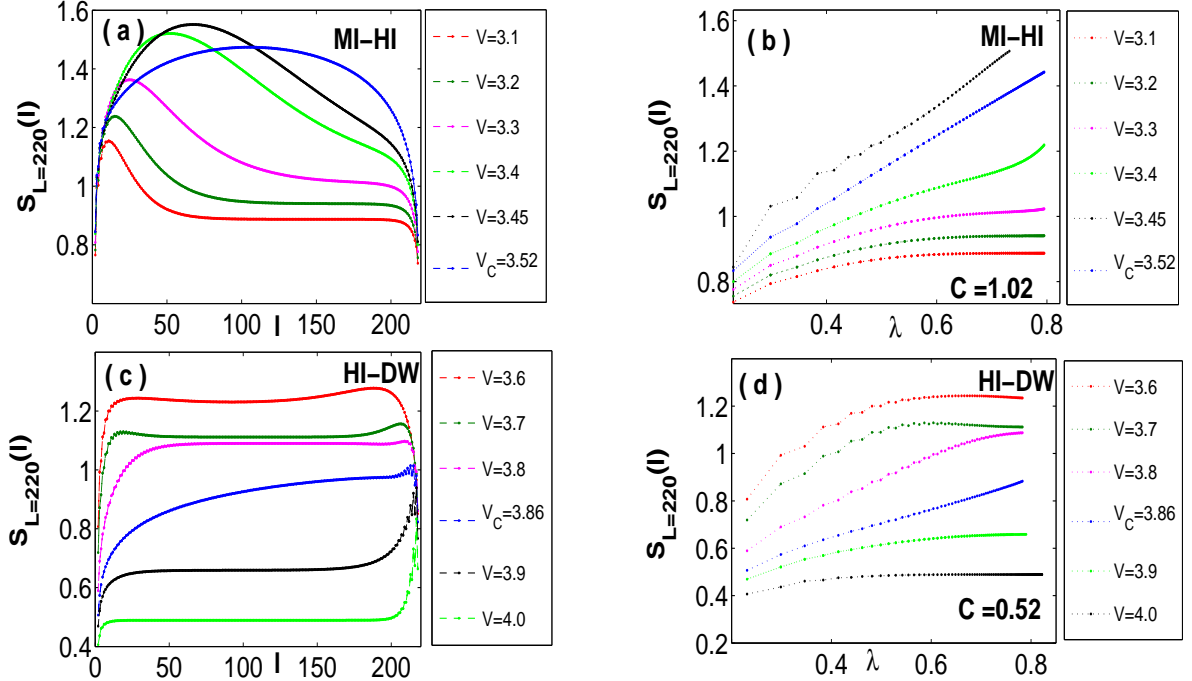


FIG. 12. (Color online) Left panels (a) and (c): the static von Neumann block entropy $S_L(l)$ for an open system of length $L = 220$ and a range of different interaction values V , located in the MI-HI and the HI-DW phases. Right panels (b) and (d): the same block entropies as a function of the logarithmic conformal distance $\frac{1}{6}\log[(2L/\pi)\sin(\pi l/L)]$; the linear behaviors of the curves for $V = 3.52$ and 3.86 reveals critical points with $c \sim 1$ and $c \sim 0.5$. The rapid saturation of the entropy for other values of V is a consequence of the short correlation length in the MI and HI insulating phases. Here the average filling is 1 and we use the constraint T3.

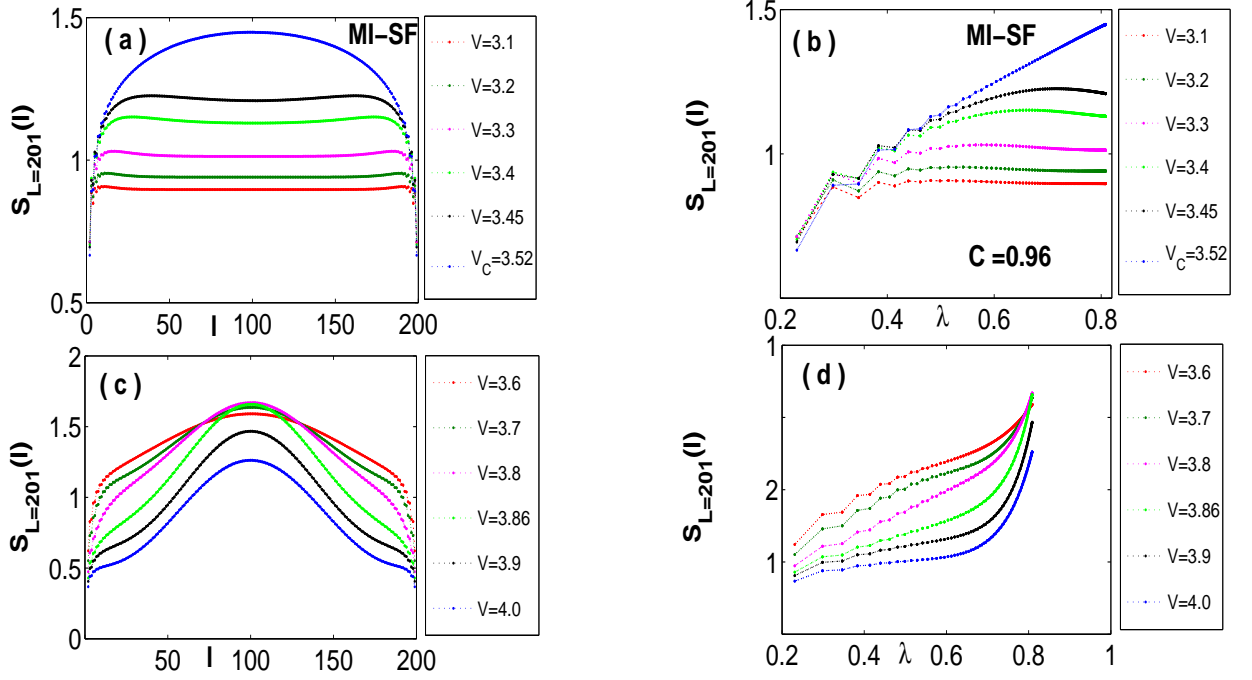


FIG. 13. (Color online) Left panel (a): the static von Neumann block entropy $S_L(l)$ for an open system of length $L = 201$ and a range of different interaction values V , located in the MI and the SF phases. Right panels (b): the same block entropies as a function of the logarithmic conformal distance $\frac{1}{6}\log[(2L/\pi)\sin(\pi l/L)]$; the linear behaviour of the curve for $V = 3.52$ reveals a critical point with central charge $c \sim 1$. The rapid saturation of the entropy for other values of V is a consequence of the short correlation length in the MI insulating phase. Here the average filling is 1 and we use the constraint T1; (c) and (d) show analogs of the plots in (a) and (b), respectively, in a parameter range with no continuous transitions.

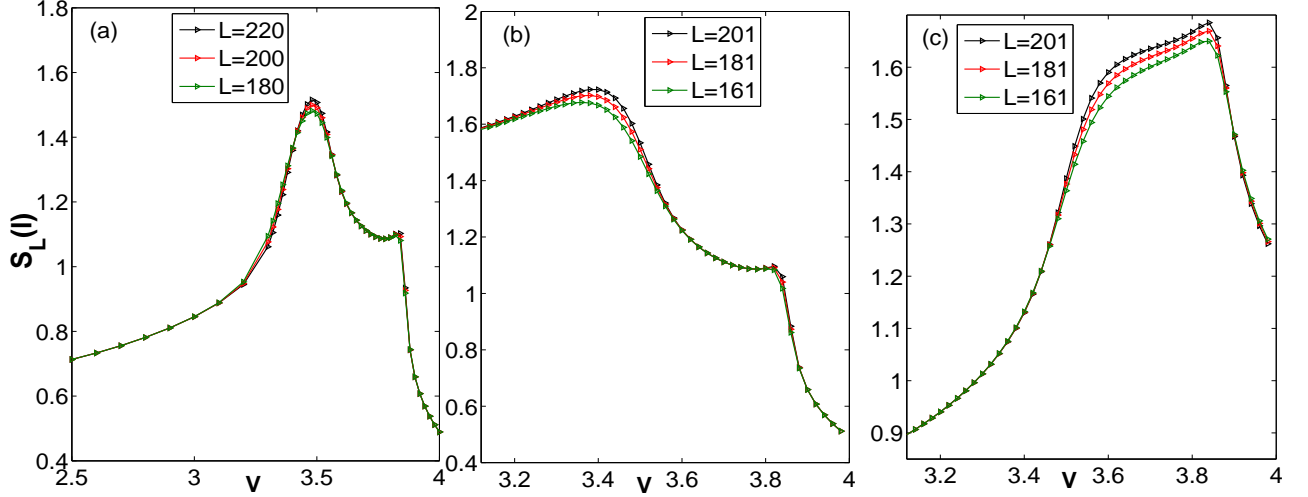


FIG. 14. (Color online) In (a) we show the entanglement entropy as a function of V ($l = L/2$); as $L \rightarrow \infty$, this shows a jump close to the Gaussian critical point $V \sim 3.52$, and, in this limit, the curves for different values of L , i.e., 220 (black line), 200 (red line), and 180 (green line), converge to a step function at the 2D-Ising-type critical point at $V \simeq 3.84$; we use the constraint T3. (b) and (c) show the analogs, for the constraints T2 and T1, respectively, of the plot (a) for different lengths L 201 (black line), 181 (red line), and 161 (green line); note the convergence to a step function, as L increases, at the 2D-Ising-type critical point $V \simeq 3.84$.

IV. CONCLUSIONS

We have performed the most extensive DMRG study of the 1D EBHM attempted so far. Our work, which extends earlier studies [6, 7, 9, 10] significantly, has been designed to investigate the effects of filling and boundary states on the phase diagram of this model, to elucidate the natures of the phase transitions here, and to identify the universality classes of the continuous transitions. Our study shows that the HI-DW, MI-HI, and SF-MI transitions are, respectively, in the 2D Ising, Gaussian, and BKT universality classes; however, the SF-HI transition seems to be more exotic than a BKT transition in so far as the string order parameter also vanishes where the SF phase begins. We find that the different constraints T1, T2, and T3, which lead to the same value of ρ in the thermodynamic limit, yield different phase diagrams; this dependence deserves more attention than it has received so far, especially from the point of view of the existence of thermodynamic limits [16]; a few six-vertex models, which are known in the statistical mechanics of two-dimensional models, can show such a boundary-condition dependence in their bulk phase diagrams as has been shown analytically in [35]. Constraints analogous to the ones that we use have been employed in studies of integer spin chains in Ref.[27]. We are not aware of any study of 1D EBHM that compares the constraints T1, T2, and T3. The studies of Ref.[6] use the constraint T1 and, therefore, find the phases SF, DW and MI. Ref.[15] employs constraint T3 and, therefore, obtain the phases SF, DW, MI and HI and Ref.[7] for the same constraint obtain the phases SF, DW, MI, HI and SS. A short version of our study is available at [30].

We hope our work will stimulate more theoretical and experimental studies of the 1D EBHM and experimental realizations thereof.

V. ACKNOWLEDGEMENT

We thank DST, UGC, CSIR (India) for support and E. Berg, E. G. Dalla Torre, F. Pollmann, E. Altman, A. Turner, V. Korepin and T. Mishra for useful discussions. RVP and JMK thank, respectively, the Indian Institute of Science, Bangalore and the Goa University, Goa for hospitality.

VI. APPENDIX: FSDMRG CALCULATIONS

The Finite-size DMRG (FSDMRG) method has proven to be very useful in studies of one-dimensional quantum systems [31–33]. We summarize below the salient features of this method. Open boundary conditions are preferred in this method because the loss of accuracy, with increasing system size is much less, with these boundary conditions than in the case of periodic boundary conditions. The conventional FSDMRG method consists of

the following two steps:

1. The infinite-system, density-matrix renormalization group (DMRG) method, with which we start, with a system of four sites, add two sites at each step of the iteration, and then continue until we obtain a system with the desired number L of sites.
2. The finite-system method in which the system size L is held fixed, but the energy of a target state is improved iteratively by a sweeping procedure, which we describe below, until convergence is obtained.

We now follow closely the discussion in Ref.[6].

For a model like the one we consider, we first construct the Hamiltonian matrix of the superblock configuration $B_1^l \bullet \bullet B_1^r$, where B_1^l and B_1^r represent left- and right-block Hamiltonians, respectively; each one of the \bullet represents a single-site Hamiltonian. In the first step of the DMRG iteration, both B_1^l and B_1^r also represent single sites, so, at this step, we have a four-site chain. We now diagonalize the Hamiltonian matrix of the superblock and obtain the energy and the eigenfunction of a target state. In our study the *target state* is the ground state of the system of size L , with either $N = L$ or $N = L \pm 1$ bosons; the latter is required, e.g., for obtaining the gap in the energy spectrum. Next, we divide the superblock into two equal halves, the left and the right parts, which are treated, respectively, as the *system* and the *environment*. The density matrix for this *system*, namely, $B_2^l \equiv B_1^l \bullet$, is calculated from the *target state*. If we write the *target state* as $|\psi\rangle = \sum_{i,j} \psi_{i,j} |i\rangle |j\rangle$, where $|i\rangle$ and $|j\rangle$ are, respectively, the basis states of the *system* and the *environment*, then the density matrix for the *system* has elements $\rho_{i,i'} = \sum_j \psi_{i,j} \psi_{i',j}$. The eigenvalues of this density matrix measure the weight of each of its eigenstates in the target state. The optimal states for describing the system are the ones with the largest eigenvalues of the associated density matrix. In this first step of the DMRG the superblock, and hence the dimension of the density matrix, is small, so all the states can be retained. In subsequent steps, however, when the sizes of the superblocks and density matrices increase, only the most significant states are retained, e.g., the ones corresponding to the largest M eigenvalues of the density matrix (we choose $M = 128$ or 256). We then obtain the effective Hamiltonian for the *system* B_2^l in the basis of the significant eigenstates of the density matrix; this is used, in turn, as the left block for the next DMRG iteration. In the same manner we obtain the effective Hamiltonian for the right block, i.e., $B_2^r \equiv \bullet B_1^r$. In the next step of the DMRG we construct the Hamiltonian matrix for the superblock $B_2^l \bullet \bullet B_2^r$, so the size of the system increases from $L = 4$ to $L = 6$. For a system of size L , we continue, as in the first step, by diagonalizing the Hamiltonian matrix for the configuration $B_{(L/2)-1}^l \bullet \bullet B_{(L/2)-1}^r$ and setting $B_{L/2}^l \equiv B_{(L/2)-1}^l \bullet$ and $B_{L/2}^r \equiv \bullet B_{(L/2)-1}^r$ in the next step of the DMRG iteration. Thus, at each DMRG step,

the left and right blocks increase in length by one site and the total length L of the chain increases by 2.

In the infinite-system DMRG method sketched above, the left- and right-block bases are not optimized in the following sense: The DMRG estimate for the target-state energy, at the step when the length of the system is L , is not as close to the exact value of the target-state energy for this system size as it can be. It has been found that the FSDMRG method overcomes this problem [32]. In this method we first use the infinite-system DMRG iterations to build up the system to a certain desired size L . The L -site superblock configuration is now given by $B_{(L/2)-1}^l \bullet \bullet B_{(L/2)-1}^r$. In the next step of the FSDMRG method, the superblock configuration $B_{(L/2)}^l \bullet \bullet B_{(L/2)-2}^r$, which clearly keeps the system size fixed at L , is used. This step is called *sweeping* in the right direction since it increases (decreases) the size of the left (right) block by one site. For this superblock, the *system* is $B_{L/2}^l \bullet$, the *environment* is $\bullet B_{(L/2)-2}^r$, the associated density matrix can be found, and from its most significant states the new effective Hamiltonian for the left block, with $[(L/2) + 1]$ sites, is obtained. We sweep again, in this way, to obtain a left block with $[(L/2) + 2]$ sites and so on until the left block has $(L - 3)$ sites and the right block has 1 site, so that, along with the two sites between these blocks, the system still has size L ; or, if a preassigned convergence criterion for the target-state energy is satisfied, this sweeping can be terminated earlier. Note that, in these sweeping steps, for the right block we need B_L^r to B_{L-3}^r , which we have already obtained in earlier steps of the infinite-system DMRG. Next we sweep leftward; the size of the left (right) block decreases (increases) by one site at each step. Furthermore, in each of the right- and left-sweeping steps, the energy of the target state decreases systematically until it converges.

We use a slightly modified form of the FSDMRG method in which we sweep, as described above, at every step of the DMRG scheme and not only in the one that corresponds to the largest value of L . Since the superfluid phase in models such as our model, in $d = 1$ and at $T = 0$, is critical and has a correlation length that diverges with the system size L , finite-size effects must

be removed by using finite-size scaling. For this purpose, the energies and correlation functions, obtained from a DMRG calculation, should have converged properly for each system size L . It is important, therefore, that we use the FSDMRG method as opposed to the infinite-system DMRG method, especially in the vicinities of continuous phase transitions. We find that convergence, to a specified accuracy for the target-state energy, is faster in the MI phase than in the SF phase.

The bases of left- and right-block Hamiltonians are truncated by neglecting the eigenstates of the density matrix corresponding to small eigenvalues; this leads to truncation errors. If we retain M states, the density-matrix weight of the discarded states is $P_M = \sum_{\alpha=1}^M (1 - \omega_\alpha)$, where ω_α are the eigenvalues of density matrix. P_M provides a convenient measure of the truncation errors. We find that these errors depend on the order-parameter correlation length in a phase. For a fixed M , we find very small truncation errors in the MI and DW phases; these grow as the MI-SF and DW-SF transitions are approached, and the truncation errors are largest in the SF phase. In our calculations we choose M such that the truncation error is always less than 5×10^{-6} ; we find that the values of M , mentioned in the main part of this paper, suffice.

The number of possible states per site in the Bose-Hubbard model is infinite, because there can be any number of bosons on a site. In a practical DMRG calculation, we must restrict the number n_{max} of states or bosons allowed per site. The smaller the interaction parameters U and V , the larger must n_{max} be. As in earlier calculations [31, 33] on related models, we find that $n_{max} = 4$ is sufficient for the values of U and V considered here; we have checked in representative cases that our results do not change significantly if $n_{max} = 5$.

In summary, then, our FSDMRG procedure gives us the energy $E_L(N)$ for the ground state of this model and the associated eigenstate $|\psi_{0LN}\rangle$. Given these, we can calculate the energy gaps, order parameters, and correlation functions that characterize all the phases of this model and thence the phase diagram.

-
- [1] I. Bloch, J. Dalibard, and W. Zwerger, Rev. Mod. Phys. **80**, 885 (2008); M. Lewenstein, A. Sanpera, V. Ahufinger, B. Damski, A. Sen(De) and U. Sen, Adv. in Physics, **56** 243 (2007).
 - [2] M.P.A. Fisher, P.B. Weichman, G. Grinstein and D.S. Fisher, Phys. Rev. B **40**, 546 (1989).
 - [3] K. Sheshadri, H. R. Krishnamurthy, R. Pandit and T. V. Ramakrishnan, Europhys. Lett. **22** 257 (1993).
 - [4] D. Jaksch, C. Bruder, J. I. Cirac, C. W. Gardiner and P. Zoller, Phys. Rev. Lett. **81**, 3108 (1998); M. Greiner, O. Mandel, T. Esslinger, T.W. Hänsch and I. Bloch, Nature (London) **415**, 39 (2002).
 - [5] T. Kühner and H. Monien, Phys. Rev. B **58**, R14741 (1998).
 - [6] R.V. Pai and R. Pandit, Phys. Rev. B, **71**, 104508 (2005); Proceedings of the Indian Academy of Sciences (Chemical Science) **115**, Nos. 5-6, 721 (2003).
 - [7] X. Deng and L. Santos, Phys. Rev. B **84**, 085138 (2011).
 - [8] J.M. Kurdestany, R.V. Pai, and R. Pandit, Ann. Phys. (Berlin) **524** No. 3-4, 234 (2012).
 - [9] E.G. Dalla Torre, E. Berg, and E. Altman, Phys. Rev. Lett. **97**, 260401 (2006).
 - [10] E. Berg, E.G. Dalla Torre, T. Giamarchi, and E. Altman, Phys. Rev. B, **77**, 245119 (2008).

- [11] D. Kovrizhin, G.V. Pai, and S. Sinha, Europhys. Lett. **72**, 162 (2005); A.F. Andreev and I.M. Lifshitz, Sov. Phys. JETP, **29**, 1107 (1969); A.J. Leggett, Phys. Rev. Lett. **25**, 1543 (1970); G. Chester, Phys. Rev. A **2**, 256 (1970); E. Kim and M.H.W. Chan, Nature **427**, 225 (2004).
- [12] J. Werner, A. Griesmaier, S. Hensler, J. Stuhler, and T. Pfau, Phys. Rev. Lett. **94**, 183201 (2005).
- [13] K. Göral, L. Santos and M. Lewenstein, Phys. Rev. Lett. **88**, 170406 (2002).
- [14] X. Deng, R. Citro, E. Orignac, A. Minguzzi, and L. Santos (2012) arXiv:1203.0505v1.
- [15] D. Rossini and R. Fazio, New Journal of Physics **14**, 065012 (2012).
- [16] D. Ruelle, *Statistical Mechanics: Rigorous Results* (Imperial College Press and World Scientific, London and Singapore, 1999); O. Bratelli and D.W. Robinson, *Operator Algebras and Quantum Statistical Mechanics 2* (Springer Verlag, Berlin, 2002).
- [17] F.D.M. Haldane, Phys. Lett. **93A**, 464 (1983); Phys. Rev. Lett. **50**, 1153 (1983).
- [18] S. M. Girvin and D. P. Arovas, Phys. Scr. **T 27** 156 (1989).
- [19] T. Kennedy and H. Tasaki, Phys. Rev. B **45**, 304 (1992).
- [20] F. Pollmann, E. Berg, A. M. Turner and M. Oshikawa, Phys. Rev. B **85**, 075125 (2012).
- [21] T. Senthil, A. Vishwanath, L. Balents, S. Sachdev and M. P. A. Fisher, Science **303**, 1490 (2004).
- [22] S. Hu, B. Normand, X. Wang and L. Yu, Phys. Rev. B **84**, 220402(R) (2011).
- [23] A. Luther and D. J. Scalapino, Phys. Rev. B **16**, 1153-1163 (1977).
- [24] J.B. Kogut, Rev. Mod. Phys. **51**, 4 (1979).
- [25] We use the conventional terminology charge gap even though we do not have charged bosons in mind. Indeed, some authors refer to our DW phase as a CDW phase.
- [26] Andreas M. Lühli and C. Kollath, J. Stat. Mech. 2008 P05018.
- [27] Steven R. White and David A. Huse, Phys. Rev. B **48**, 3844 (1993).
- [28] R. Shankar and N. Read, Nucl. Phys. B **336**, 457 (1990).
- [29] C. Itoi and M-H. Kato, Phys. Rev. B **55**, 8295 (1997).
- [30] J.M. Kurdestany, R.V. Pai, S. Mukerjee, and R. Pandit, to be published.
- [31] R. V. Pai, R. Pandit, H. R. Krishnamurthy, and S. Ramasesha, Phys. Rev. Lett. **76**, 2937 (1996).
- [32] S. R. White, Phys. Rev. Lett. **69**, 2863 (1992); Phys. Rev. B **48**, 10345 (1993).
- [33] R. V. Pai and R. Pandit, Proc.-Indian Acad. Sci., Chem. Sci. **115**, 721 (2003).
- [34] U. Schollwöck, Rev. Mod. Phys., **77**, (2005).
- [35] V. Korepin and P. Zinn-Justin Journal of Physics A **33**, 7053 (2000); P. Zinn-Justin Phys. Rev. E **62**, 3411 (2000).